MS #32579

Feb 28, 2007
Manuscript after minor revision

Material names (#32579):

Silicon

Silicon nitride

Carbon

Quartz

Robax

Keywords (#32579):

Wafer temperature

Radiative heating

IR emitters

Spectral absorption

Spectral emissivity

surface roughness

Plasma deposition

PECVD

Silicon

Silicon nitride

Carbon

Quartz

Robax

Radiative wafer heating during plasma deposition process

R.C.M. Bosch, C.H. Kant, A.J.M. van Erven, W.T.M. Stals, and M.D. Bijker

OTB Solar, Luchthavenweg 10, 5657 EB Eindhoven, Netherlands

Wafer heating with visible and infrared radiation is a well established method used in plasma deposition reactors used for solar cell production. A detailed study on radiative heat transfer as presented in this paper gives a quantitative description by considering the spectral absorption of radiation in optical components, contamination of these components during plasma growth, the spectral emissivity of the silicon solar cell and the effect of heat buffer components. Even with a clever implementation of heaters the net power incident on the wafer is shown to decrease to 60%. The wafer temperature ramp up time is shown to be dependent on the surface roughness and dopant level of the silicon solar cell, whereas the steady-state temperature during plasma growth is independent on these properties. Due to contamination during plasma growth, the wafer temperature decreases with 80K within one production shift, but this decrease can be minimized to 10-20K by implementing heat buffer components.

5275Rx, 8115Gh, 4320Rz, 4440+a, 5225Rv, 6180Az, 6180Ba, 9410Gb

I. Introduction

In many industrial plasma deposition tools used for solar cell fabrication the wafer temperature is stabilized by radiative heating. Equipment design is often optimized on throughput and yield, whereas process quality is measured by solar cell efficiency at the end of the production line, or

by optical properties of the plasma deposited layer. As a consequence, the efficiency of radiative heat transfer is often neglected, and, more importantly, long term process stability with respect to the wafer temperature profile is difficult to maintain. This paper gives a detailed model on the physics involved in radiative heat transfer from the heaters to the wafer, considering the spectral absorption of optical elements, heating and re-emission of these components, reactor contamination and the spectral absorption and emission of a silicon wafer that strongly depends on doping concentration, wafer temperature and surface properties. The calculations are compared to in-situ wafer temperature measurements.

II. Implementation of radiative heaters

Figure 1 shows an example of radiative wafer heating. The vacuum chamber is part of the DEPx system, which is used for plasma deposition of silicon nitride on solar cells [5-9]. The deposition process is dynamic: the wafer is transported with constant velocity through a pre-heat zone for temperature ramp up, and through a plasma deposition zone. The used heaters are short-wave infrared emitters with a maximum power of 4800W, and a filament temperature of 2650K at maximum power and 2238K at 50% of maximum power [1].

The infrared heaters are inserted in quartz tubes. At the same time, the tubes also act as a vacuum sealing, so that the heaters can easily be exchanged (see Fig. 2). The quartz tubes show good optical transparency in the range of 0.3 to 5 micron, therefore minimizing heat losses. As the outside surface of the quartz tubes is exposed to plasma deposition, the tubes need to be protected from contamination. This is done by implementing glass shielding plates inside the vacuum (see

Figure 3). As the glass plates become contaminated during production, they can be daily exchanged. Robax™ is used as a glass type because of its good optical transparency.

The corresponding optical absorption is shown in Fig. 4. It can also be seen that the absorption of Robax increases during production. In the range between 1 and 3 micron, the absorption of Robax increases from nearly zero (clean) to 0.92 (fully covered with silicon nitride after two days).

III. Radiative heat transfer model

Figure 3 illustrates the method of wafers heating in the DEPx system. The heater emits the radiation both upwards towards the top reflector, where it is partially reflected (reflection coefficient R_1), and absorbed (absorption coefficient A_1), and downwards towards the wafer. As the top reflector is heated, additional radiation will be emitted that can be described by a grey body spectrum at the corresponding temperature (see section IV).

The quartz tube will also reflect, absorb and re-emit radiation in the same way (R_2, A_2), just as the Robax glass plate (R_3, A_3). The latter will also be coated with a silicon nitride layer during plasma growth, and will increasingly absorb radiation during production (A_4).

The resulting radiation is partially absorbed by the wafer (A_5). Part of the radiation will be reflected at the wafer, thereby heating the stainless steel reactor wall shielding. As a result, the shielding will also be heated and emit radiation back into the reactor. The wafer is put on a fiber glass carbon wafer plate that acts as a heat buffer for temperature stabilization.

IV. Radiation spectrum

The power density of the IR emitter can be accurately described by Planck's law:

$$P_0(\lambda) = \varepsilon_0(\lambda) \cdot \frac{2\pi c^2 h}{\lambda^5} \frac{1}{\exp[hc/(k\lambda T_0)] - 1} \quad (1)$$

with $\varepsilon_0(\lambda)$ the spectral emissivity of the tungsten filament at temperature T_0, c the velocity of radiation ($3.0 \cdot 10^8$ m/s), h Planck's constant ($6.6 \cdot 10^{-34}$ Js), k Boltzmann's constant ($1.6 \cdot 10^{-23}$ J/K), and λ the wavelength of the radiation. Under standard heating conditions, the filament temperature T_0 is in the range of 2200 to 2300 K, and the maximum power is around a wavelength of $\lambda \approx 1.2$ µm. The integrated radial power density over wavelength gives the total power of the radiation (W/m^2):

$$P_0 = \int_0^\infty P_0(\lambda) d\lambda = \varepsilon_0 \sigma T_0^4 \quad (2)$$

with ε_0 the average emissivity (definition of emissivity for a grey body), and σ Stefan-Boltzmann's constant ($5.67 \cdot 10^{-8}$ $W/m^2/K^4$).

Part of the radiation will reach the substrate directly; the remaining part is either absorbed in the optical components or directed in the opposite direction due to reflections. The absorbed radiation of not entirely lost: since the quartz tube and Robax glass plate will heat up significantly, these components will re-emit radiation both towards and away from the substrate.

In general, the total spectrum towards the wafer is therefore a sum of the filtered spectrum of the IR emitter $f_0(\lambda)\cdot P_0(\lambda)$, the spectrum of the re-emitting top reflector $f_1(\lambda)\cdot P_1(\lambda)$, re-emitting quartz tube $f_2 \cdot P_2(\lambda)$ and re-emitting Robax glass plate $f_3 \cdot P_3(\lambda)$:

$$\left.\begin{aligned} &P_{total}(\lambda) = f_0(\lambda)\cdot P_0(\lambda) + f_1(\lambda)\cdot P_1(\lambda) + f_2\cdot P_2(\lambda) + f_3\cdot P_3(\lambda) \\ &f_0(\lambda) = \frac{1}{2}(1+R_1)(1-R_2)^2(1-R_3)^2(1-A_2(\lambda))(1-A_3(\lambda))(1-A_4) \\ &f_1(\lambda) = \frac{1}{2}(1-R_2)^2(1-R_3)^2(1-A_2(\lambda))(1-A_3(\lambda))(1-A_4) \\ &f_2(\lambda) = \frac{1}{2}(1-R_3)^2(1-A_3(\lambda))(1-A_4) \\ &f_3 = \frac{1}{2} \end{aligned}\right\} \quad (3)$$

The term $(1+R_1)$ in $f_0(\lambda)$ arises from the reflection of the filament's radiation in the top reflector. Second order effects (absorption of re-emitted power from one component in the other) can be neglected for this purpose.

The emitted power of the top reflector $P_1(\lambda)$ equals that of a grey body (see Eq. (1)) with an emissivity $\varepsilon_1 = 1 - R_1 = 0.6$ which is independent of wavelength [1] and a temperature T_1. Its temperature can be determined by the amount of absorption from the heater:

$$\frac{1}{2}(1-R_1)\cdot P_0 = \varepsilon_1 \sigma T_1^4 \quad (4)$$

It is more complex to determine the radiation spectrum of the quartz and Robax components since the corresponding spectral emissivities $\varepsilon_2(\lambda)$ and $\varepsilon_3(\lambda)$ are dependent on wavelength.

According to Kirchhoff's law, the spectral emissivities are equal to the spectral absorptions $A_2(\lambda)$ and $A_3(\lambda)$ as measured in Fig. 4. As a result, the radiation spectrum of quartz can be written as follows:

$$P_2(\lambda) = c_2 \cdot \varepsilon_2(\lambda) \cdot \frac{2c^2 h}{\lambda^5} \frac{1}{\exp[hc/(k\lambda T_2)] - 1} \quad (5)$$

where the constant c_2 and quartz temperature T_2 are derived by conservation of energy: the integrated power of $P_2(\lambda)$ equals the absorbed power from the radiation of the heaters:

$$\int_0^\infty \frac{1}{2}(1+R_1)(1-R_2)P_0(\lambda)A_2(\lambda)d\lambda = \int_0^\infty P_2(\lambda)d\lambda = \varepsilon_2 \sigma T_2^{\,4} \quad (6)$$

Here the average emissivity of quartz ε_2 is equal to 0.5 [1]. The spectrum $P_3(\lambda)$ emitted by the heated Robax glass plate can be derived in the same way:

$$\int_0^\infty \frac{1}{2}(1+R_1)(1-R_2)^2(1-R_3)P_0(\lambda)[A_3(\lambda) + A_4 - A_3(\lambda) \cdot A_4]d\lambda = \int_0^\infty P_3(\lambda)d\lambda = \varepsilon_3 \sigma T_3^{\,4} \quad (7)$$

The term $A_3(\lambda) + A_4 - A_3(\lambda) \cdot A_4$ represents the total absorption in the Robax glass plate with silicon nitride contamination layer, which can be deduced from

$$A = 1 - T = 1 - (1 - A_3(\lambda)) \cdot (1 - A_4) \quad (8)$$

where A represents the total absorption and T the total transmission. Figure 4 shows the measured values of the total absorption. The absorption of the silicon nitride layer A_4 can be estimated by comparing with the measured values of a clean Robax glass plate ($A_4 = 0$). It can be seen that after one day of production the absorption has significantly increased ($A_4 = 0.8$), and after two days the absorption is 1.0 over the entire spectrum.

Figure 5 shows examples of the calculated spectra due to reflection, absorptions and re-emission. In this case, the lamp setting is set to 50% of maximum power, resulting in a filament temperature of 2238K. For a clean system, the net power decreases to 60%. In case of plasma deposition, the Robax glass plates become contaminated and the deposited silicon nitride layer will also start to absorb radiation. It can be seen that for total covering of silicon nitride on Robax, which corresponds to an absorption coefficient of $A_4 = 1.0$, the spectrum is severely altered towards the infrared. All the radiation in the range of 1 to 2 micron, which is the main component of the lamp spectrum, is fully absorbed. The net power incident on the wafer has decreased to 35%.

In case another heater type is used for wafer heating with a different filament temperature, one has to consider a different absorption in the optical components used in the system. Fig. 6 illustrates this effect. It can be seen that a higher filament temperature gives a better heating efficiency. Also, the comparison of Robax with another glass type as borosilicate is shown. By using Robax the heating efficiency is about 5% higher, corresponding to a relative increase of 10 to 15%.

V. Spectral absorption and emissivity of silicon

The early work of Sato *et al.* [3] has shown that the emissivity of a silicon wafer depends greatly on wavelength, doping level and temperature. At room temperature and low doping level (< 10E14 per cm^3), the absorption or emissivity is highest for radiation below 1.1 micron, corresponding to photon energies exceeding the band gap energy of silicon (1.1 eV). The paper of Ravindra *et al.* [2] continues this work with emissivity/absorption measurements at different doping levels, and the paper of Sopori *et al.* [4] considers the effects of surface roughness and various coatings. Figure 7 shows the corresponding measurements performed by Ravindra *et al.* At room temperature the emissivity or absorption is highest at a wavelength below 1.1 micron. However, this trend disappears gradually at an increasing wafer temperature. It can be seen that the absorption will eventually become almost independent of the wavelength as the wafer temperature increases to 700°C.

The absorbed radiation power can be calculated by taking the convolution of the spectral absorption and the radiation spectrum. Since the wavelength region between 1 and 2 micron is most abundant in the radiation spectrum (see Fig. 5), the absorption of the heater's radiation is greatly dependent on the wafer temperature. For example, the total absorption is 0.2 at room temperature and increases to 0.5 at 500°C.

The emitted radiation power is obtained from a convolution of the spectral absorption (emission) and the radiation spectrum from a black body at the corresponding wafer

temperature. It can also be estimated by taking the emissivity value at the wavelength of maximum power of a black body at the corresponding wafer temperature according to Wien's law. The wavelength of maximum power is shown in Fig. 7.

The emissivity as shown in Fig. 7 is measured on a double sided polished (DSP) wafer. In solar cell processing, wafer surface is often textured, introducing a reduction in the average reflection and an increase in emissivity [4]. As a rule of thumb, the average reduction in reflectivity is equal to the average increase in emissivity. For acid etched wafers the reflection decreases from 0.3 to 0.25, and for alkali etched wafers the reflection can even decrease down to 0.10, causing the emissivity at 1.0 micron to increase to 0.9. Furthermore, during plasma deposition of an anti-reflection layer of silicon nitride, the reflection is reduced from 0.3 to 0.1 on DSP wafers, resulting in a similar increase in emissivity. These effects are taken into account in the heat model that is described in section III.

VI. Comparison of the heat model results with measurements

Figure 8 shows the measured and calculated temperature of the top reflector. There is a good agreement, especially at a higher reflector temperature. This indicates that convective heat transfer (the heater is mounted in the ambient, not in vacuum) can be neglected in this range. However, the disagreement between the measured value and calculated value at low power can increase up to 100K, as in this case the heat transfer is dominated by air convection.

The wafer temperature in the DEPx is measured in-situ with a thermal data collector (Datapaq). These values are compared to the results of the model. During pre-heat the wafer will heat up with a rate depending on the corresponding absorption as shown in Fig. 7. Table I shows the results of the comparison.

Figure 9 shows the steady-state temperature during plasma deposition of different wafers types as a function of radiation power. It can be seen that a steady-state wafer temperature of more than 500°C can be achieved using 80% of maximum heating power. It can also be seen that the wafer temperature increases almost linear with radiation power in stead of $P^{1/4}$. This is due to an increasing heating efficiency as the heaters filament temperature increases with increasing temperature (see Fig. 6).

The effect of using a heat buffer in the system is illustrated in Table II. The heat buffer is represented by a stainless steel reactor wall shielding. As also shown in Fig. 3 schematically, the shielding absorbs all the radiation that is not directly coupled into the wafer. The temperature of the shielding is determined by energy conservation: the absorbed radiation is emitted back into the reactor and towards the water cooled reactor wall. In a standard condition (2400W power per lamp, giving a net power of 1439W), the wall shield reaches a temperature of 575K. Without this shielding the wafer temperature will drop with 80K according to measurements, and 75K according to the model. Using a double walled shielding, the wafer temperature will increase with 25K (measured), or 13K (calculated).

Contamination of the Robax glass shielding during plasma deposition causes a severe decrease in available radiation power and causes a spectrum shift towards the infrared (see Fig. 5). As a result, a significant decrease in wafer temperature during production can be expected. As shown in Fig. 4, the Robax glass plates do not show any transmission after two days of production. Table

II shows this effect on the steady state wafer temperature during deposition. According to the calculations, the wafer temperature is expected to decrease with 80K in case the Robax glass shielding does not transmit any of the radiation. However, in practice this decrease is only 10K to 20K. This disagreement can be explained by the fact that the radiation that is emitted by the Robax plates towards the heater (which is considered as lost) is partially reflected at the heater's top reflector back into the process chamber. This effect causes an increase in the temperature of the reactor wall shielding which is the ambient temperature of the system.

VII. Conclusions

The DEPx uses radiative heat for wafer heating during the deposition process. The short-wave infrared heaters are easily implemented in the system. The heaters remain in the ambient, while quartz tubes transmit the radiation into the vacuum.

The efficiency of the heating system is 60% by the use of highly optical transparent components as quartz and Robax, and by using well designed heaters with a high filament temperature in the range of 2000 to 2600K. The use of Robax instead of other glass types (e.g. Borosilicate glass) increases the efficiency by 10-15% relatively.

A careful analysis of the radiative heat transfer to the wafers gives a good insight in the heating mechanisms. A lamp spectrum change due to absorption in the optical elements and heating of these components, the emissivity factor of the wafer and the use of heat buffer elements are important aspects that need consideration. During the pre-heat there appears to be a large

temperature difference for different wafer types. The steady-state temperature is much less sensitive to this.

Finally, contamination of the Robax glass shields causes a decrease in wafer temperature. In practice this decrease is quite modest (10 to 20K), probably since the main part of the radiation that is re-emitted back is scattered in the reactor and eventually absorbed in the wall shielding, raising the ambient temperature.

1234567

Table I: Temperature ramp up for different wafer surface properties. Radiation power is 1824W per lamp (38% of maximum power)

Wafer type	Calculated	Measured
Double side textured	16.5 ^{o}C/s	16.1 ^{o}C/s
Double side polished	7.5 ^{o}C/s	9.0 ^{o}C/s

Table II: Wafer temperature during plasma deposition

	shielding temperature (calculated)	net power per lamp (calculated)	wafer temperature (calculated)	wafer temperature (measured)
clean system 1	575 K	1439 W	+0	+0
no wall shielding	300 K	1439 W	- 75 K	- 80 K
double walled shielding	601 K	1439 W	+ 13 K	+ 25 K
clean system 2	537 K	1078 W	+0	+0
after two days	476 K	695 W	-80 K	-10 K to -20 K

Figure captions:

FIG. 1: DEPx PECVD process chamber with pre-heat section and deposition chamber with plasma source. During pre-heat the wafers are heated with 6 short-wave infrared emitters; during plasma deposition the wafer temperature is stabilized by 4 emitters.

FIG. 2: heating concept in the DEPx system: the IR emitters are located outside the vacuum. The quartz tubes act as a vacuum sealing, transmitting the radiation very efficiently towards the wafer.

FIG. 3: schematic representation of the radiation transport for wafer heating in the DEPx. The heaters are short-wave infrared emitters that are inserted in a quartz tube. Contamination of the tubes during plasma deposition is prevented by Robax glass plates that are mounted in the vacuum chamber. The final radiation spectrum towards the wafer is a sum of the original spectrum P_0, filtered through the quartz tube and Robax plate, and the long wave spectra from the re-emitting top reflector, quartz and Robax that are heated due to absorption of the heater's radiation P_0.

FIG. 4: optical absorption of Robax according to specifications of the suppliers (straight line), and measured optical absorption of Robax glass during production with increasing thickness of the silicon nitride layer (dotted lines). The absorption of the silicon nitride layer as expressed by A_4 is deduced from the measured value. It is also indicated in the graph.

FIG. 5: radiation spectrum change for different absorption coefficients A_4 of a silicon nitride layer on the Robax glass plates.

FIG. 6: Efficiency of the heating system used in the DEPx system as a function of the heater's filament temperature.

FIG. 7: Results of Sato and Ravindra et. al. [2,3] showing the measured emissivity of silicon (700 micron wafer, doping level 1E17 / cm^3) as a function of wavelength and temperature. The arrows indicate the wavelength of maximum emission of a grey body at the corresponding temperature.

FIG. 8: Top reflector temperature as function of power set point. The straight line represents the calculated value.

FIG.9: Simulated steady-state wafer temperature as function of input power. Markers represent measured values of different wafer types.

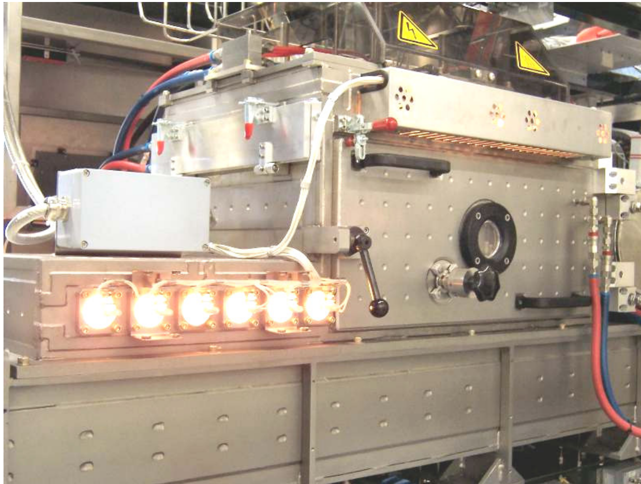

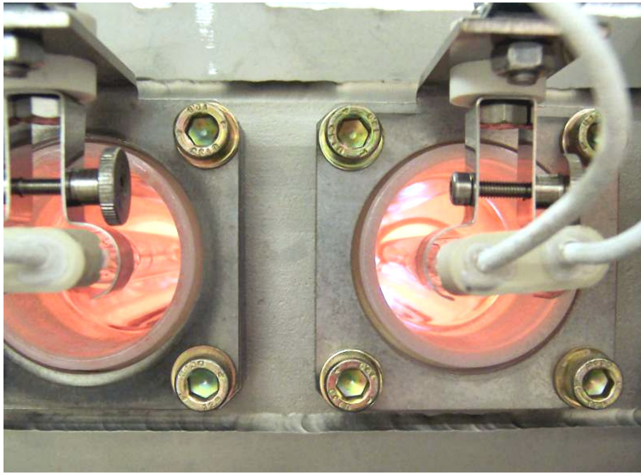

R.C.M. Bosch *et.al.*

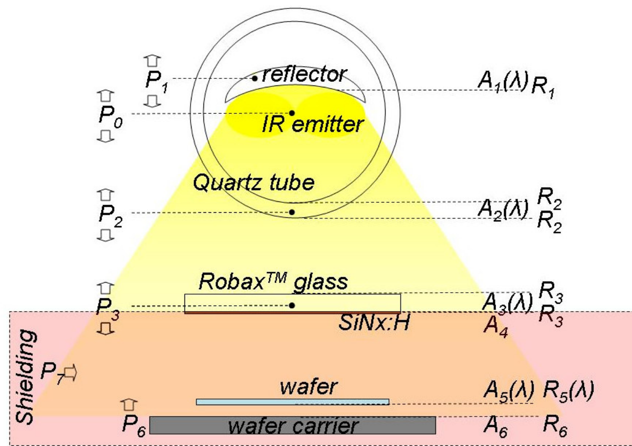

R.C.M. Bosch *et.al.*

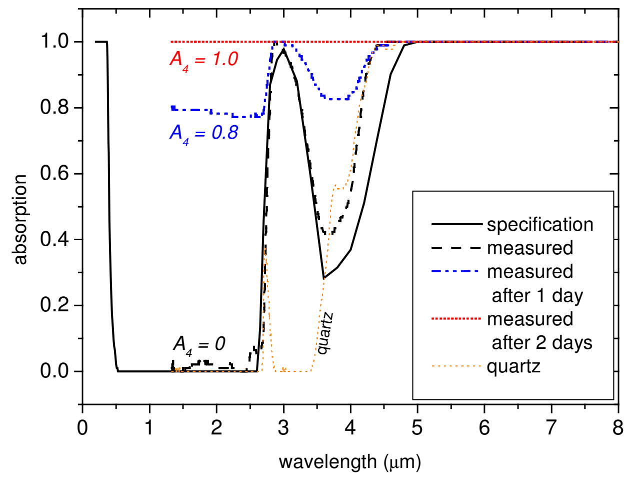

R.C.M. Bosch *et.al.*

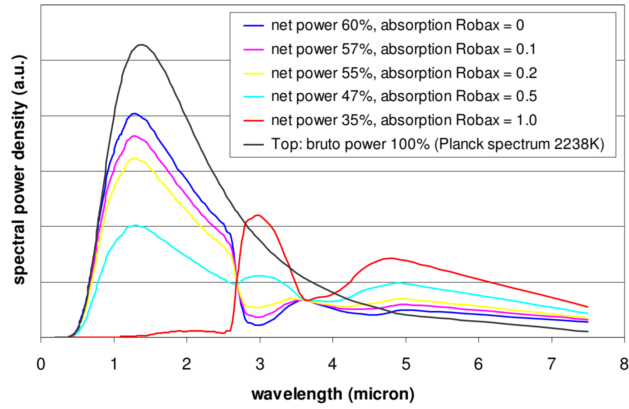

R.C.M. Bosch *et.al.*

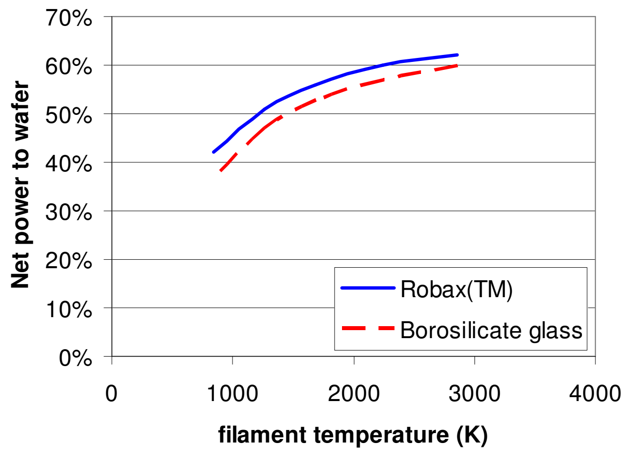

R.C.M. Bosch *et.al.*

Journal of Vacuum Science and Technology A

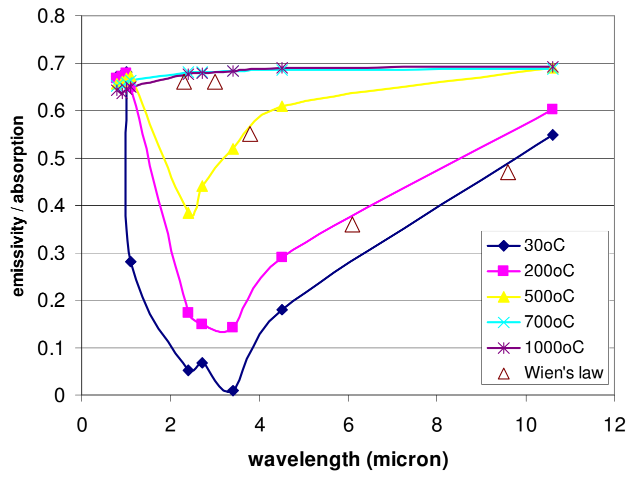

R.C.M. Bosch *et.al.*

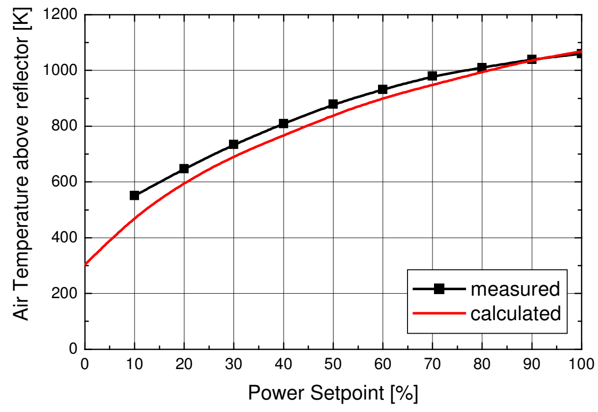

R.C.M. Bosch *et.al.*

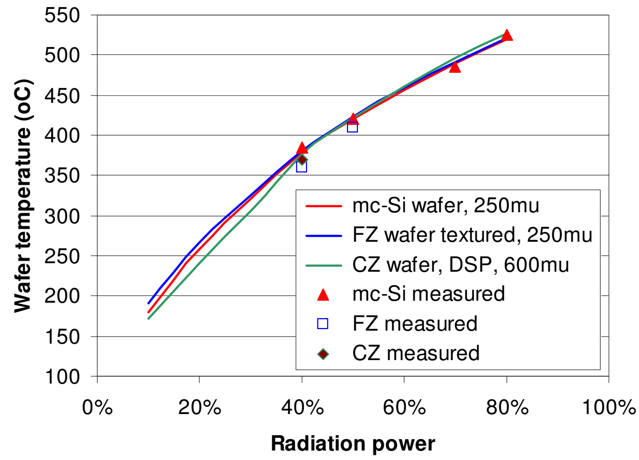

R.C.M. Bosch *et.al.*

[1] C.H. Kant, A.J.M. van Erven, R.C.M. Bosch, W.M.T. Stals, and M.D. Bijker, IEEE 4th world conference on photovoltaic energy conversion, Waikoloa, Hawaii, (2005).

[2] N.M. Ravindra, B. Sopori, O.H. Gokce, S.X. Cheng, A. Shenoy, L. Jin, S. Abedrabbo, W. Chen, and Y. Zhang, International Journal of Thermal Physics **22**, 5 (2001).

[3] K. Sato, Journal of Applied Physics **6**, 339 (1967).

[4] B. Sopori, W. Chen, J. Madjdpour, and N.M. Ravindra, Journal of Electronic Matrials **28**, 12 (1999).

[5] A.J.M. van Erven, R.C.M. Bosch, B. Hoex, M. Bennett, B. Kumar, S. Narayanan, T. Koval, and M.D. Bijker, 20th European Photovoltaic Solar Energy Conference, Barcelona, Spain, (2005).

[6] W.M.M. Kessels, P.J. van den Oever, B. Hoex, R.C.M. Bosch, A.J.M. van Erven, M.D. Bijker, and M.C.M. van de Sanden, 31st IEEE Photovoltaic Specialist Conference, Orlando, USA, (2005).

[7] A.J.M. van Erven, R.C.M. Bosch, R. Toelle, O. Voigt, S. Petri, and M.D. Bijker, 31st IEEE Photovoltaic Specialist Conference, Orlando, USA, (2005).